Nondestructive evaluation of metal contaminated silicon wafers using radiometric measurements

K. Kalli, A. Othonos, and C. Christofides[a)]
Department of Natural Sciences, Faculty of Pure and Applied Sciences, University of Cyprus, P. O. Box 537, 1678, Nicosia, Cyprus

F. Tardiff
LETI (CEA - Technologies Avancées), DMEL-CEN/G, F38054, Grenoble, Cedex 9, France

(Received 21 January 1999; accepted for publication 8 June 1999)

We have performed nondestructive measurements on metal contaminated silicon wafers using photothermal radiometric measurements. Data were collected as a function of modulation frequency and time, showing clear distinctions between the different samples examined. The sensitivity of this technique to different forms of metallic contamination is examined. A qualitative and semiquantitative comparison is made between theory and experiment. © *1999 American Institute of Physics.* [S0021-8979(99)00618-0]

I. INTRODUCTION

The processes employed to clean silicon wafers can, paradoxically, be a major source of impurities. This is particularly so in the case of metallic contamination. It is therefore important to have optimized wafer-monitoring techniques, as this is where the greatest control must be maintained. Any detection method employed must be nondestructive and noncontacting while having a high spatial resolution. We have used photothermal radiometry (PTR) as our chosen nondestructive evaluation methodology .[1–3] This approach relies on measuring the blackbody radiation emitted from a material excited by a modulated laser source. Information is recovered regarding the electronic and thermal properties of the semiconductor as a function of the laser modulation frequency. An ideal blackbody radiator produces a linear frequency spectral response. In contrast, implanted or doped silicon wafers have a frequency spectrum that is biased at lower frequencies from the thermal component and at higher frequencies by the electronic material properties. The degree of the relative contributions gives information that is dependent on the type of doping and the material characteristics.

II. THEORY

The PTR signal is divided into thermal and electronic components, the relative contributions of which determine the form of the PTR signal with a frequency[4]

$$S_{\mathrm{PTR}}(\omega)=\frac{I_0}{h\nu}\left(C_T\frac{(h\nu-E_g)}{k\sigma_t^2}+C_N\frac{1}{\sigma_n(D_n\sigma_n+s)}\right). \quad (1)$$

Here I_0 is the excitation power density, $h\nu$ the photon energy, E_g the semiconductor band gap, k the thermal conductivity, D_n and β are the minority carrier and thermal diffusivities, s the recombination velocity, τ is the minority carrier lifetime, and σ_t and σ_n are the complex thermal and plasma wave vectors, respectively. ω is the angular modulation frequency of the laser output.

$$\sigma_t=\sqrt{\frac{i\omega}{\beta}}, \quad (2a)$$

$$\sigma_n=\sqrt{\frac{1+i\omega\tau}{D_n\tau}}. \quad (2b)$$

Finally, C_T and C_N are the thermal wave and plasma wave coefficients. To gain further insight into the mechanism, one can ignore the thermal contribution and retain only the electronic contribution to $S_{\mathrm{PTR}}(\omega)$. Taking logarithms one obtains[2]

$$\log_{10}|S_{\mathrm{PTR}}(\omega)|\propto A-\log_{10}\left(\frac{1+i\omega\tau}{\tau}\right)(1+U), \quad (3)$$

where U is given by

$$U=\frac{s\tau}{L_e\sqrt{(1+j\omega\tau)}}. \quad (4)$$

A is a normalization constant and L_e is the injected carrier diffusion length equal to $(D\tau)^{1/2}$. In general, U can be ignored for the modulation frequencies of 0.1–100 kHz used here. Therefore, at low frequencies, $\omega\tau\ll 1$, and the above relation reduces to $A+\log_{10}\tau$ and is independent of ω. From this relation one can see that at low frequencies, an increase of τ leads to an increase of the photothermal radiometric signal. For high frequencies $\omega\tau\gg 1$, Eq. (3) approaches

$$A+\log_{10}[j\omega+1/\tau+(s/\sqrt{D})\sqrt{(1/\tau)+j\omega}]. \quad (5)$$

For long recombination lifetimes, for which $\omega\tau\gg 1$, Eq. (5) becomes $A+\log_{10}[j\omega+(s/\sqrt{D})\sqrt{j\omega}]$, where the slope of the curve is determined by the material parameter ratio $s/\sqrt{D}$. Conversely, for short τ, such that $\omega\tau\ll 1$, the foregoing expression becomes $A+\log_{10}(1/\tau+s/L_e)$ and the signal is independent of ω. This provides an explanation for the decrease in the PTR signal amplitude with increasing

a)Electronic mail: costasc@earth.ns.ucy.ac.cy

TABLE I. Metal contaminated silicon wafers examined using PTR.

Figure legend/ concentration	Sample Details
Fe 5×10^{12}+rec	Annealed at 950 °C dry conditions to grow a 70 Å oxide layer
Fe 5×10^{11}+rec	As above
Fe 5×10^{10}+rec	As above
Fe 5×10^{12}	Iron-doped Si wafer
Fe 5×10^{11}	As above
Fe 5×10^{10}	As above
Epi n/p^+ 5×10^{15}	Epitaxial: Wafers are p type with a superficial layer of n-type: 20 μm implanted with P at the specified concentrations
Epi n/p^+ 10^{14}	As above
Epi p/p^+ 5×10^{15}	As above, except p-type layer

contamination dosage and a decrease in the carrier lifetime. It has been shown both experimentally and theoretically[5] that the thermal and the carrier plasma wave components operate in distinct frequency regimes. The thermally dominated low frequency regime has an $\sim\omega^{-1}$ dependence. The intermediate frequency regime maintains a constant signal level that is proportional to the carrier lifetime, for samples with a low s. Finally, there is a plasma dominated high frequency regime that exhibits a frequency dependent behavior ranging from $\sim\omega^{-1}$ and $\sim\omega^{-0.5}$ for low and high s. Therefore, we may add the observed frequency dependent negative slopes of the PTR amplitude that result from the thermal wave component, to complete the understanding of the PTR frequency spectrum.

III. EXPERIMENTAL RESULTS

A. Frequency scan

All photothermal radiometric measurements have been obtained using an apparatus similar to that employed in Ref. 3. In the execution of this experiment, laser powers, from the Ar^+ laser operating at 514 nm, were kept low to avoid wafer damage (40 mW). Additionally, focusing of the laser light was relaxed in order to avoid three-dimensional diffusion effects (1 mm beam diameter). A small sample of the silicon wafers examined is listed in Table I. It should be noted that the samples did not undergo any special treatment prior to these measurements, they were kept in a dust-free environment at standard temperature and pressure until the time that the measurements were made.

Figure 1 shows the typical theoretical curves for samples that display strongly thermal, electronic (for different minority carrier lifetimes), and combined contributions. Figure 2 shows the recovered PTR amplitude signal for the P-ion implanted layers. These samples show a strong thermal content, displaying a frequency dependent negative gradient with a very small electronic contribution at high frequencies. This behavior is characterized by a linear decrease in the signal strength as a function of frequency—that the slopes between these curves are different indicates that the samples have different thermal properties. The purely thermal character of the signal is an indication of the lack of electrical activity of

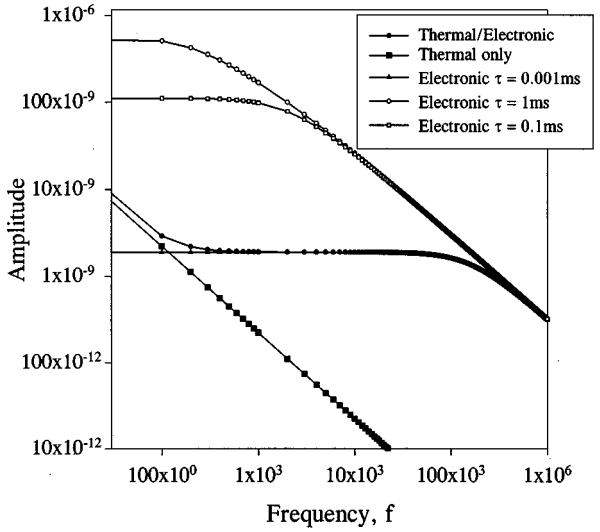

FIG. 1. Typical theoretical curves for the PTR amplitude for samples displaying various combinations of thermal and electronic behavior.

these wafers. For the purpose of comparison, we give an example of unimplanted crystalline Si. We have consistently obtained excellent reproducibility for these results that are comparable in form to earlier reports for nonannealed, P-implanted wafers.[2] We observe an increase in signal strength as the implantation dosage is increased, while the signal strength is maintained over a larger frequency range. This is a reversal in behavior to that reported in Ref. 2 for the same dosage level that we believe is related to the processing of the semiconductor and the perturbative effect of both the additional n-type overlayer and the P implantation. The implantation-induced deterioration of the near-surface thermophysical properties of the samples appears to be severe, therefore, the thermal wave centroid is localized causing an increase in the PTR signal, through the poor heat conduction to the substrate. This causes the reversal in amplitude that is due to the thermal wave intensity.

Conversely, strong electronic behavior is displayed by the different Fe-doped samples at high frequencies (above 1

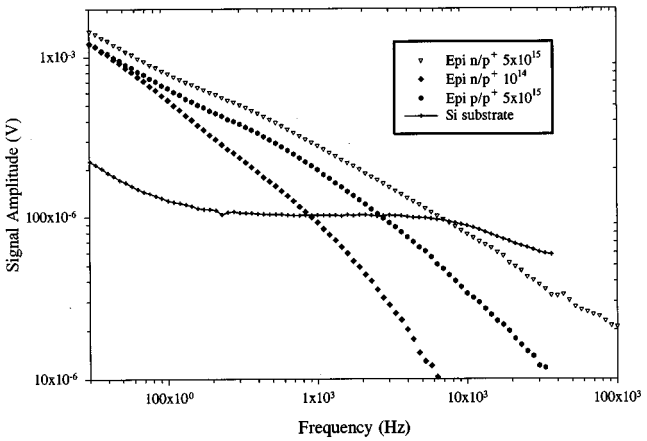

FIG. 2. PTR signal vs modulation frequency for the contaminated silicon wafers, displaying clear thermal material behavior and compared to a standard silicon substrate.

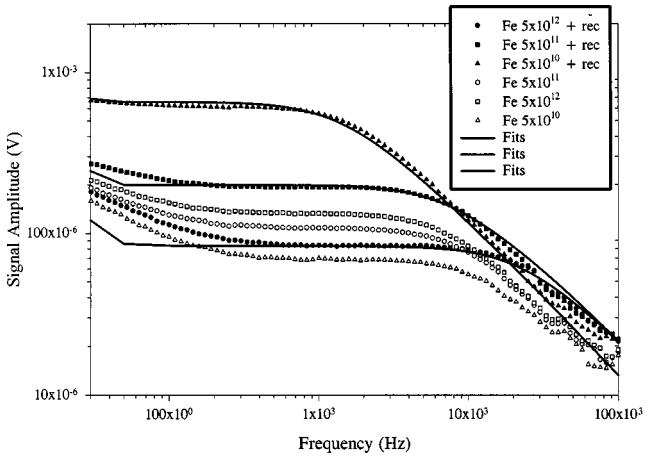

FIG. 3. PTR signal vs modulation frequency for the contaminated silicon wafers, displaying clear electronic material behavior with curves fitted according to Eq. (1).

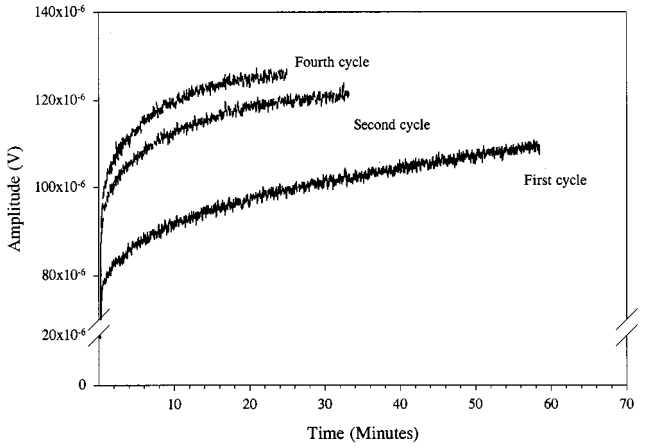

FIG. 4. Time dependent behavior of Si substrate on multiple exposure of the same point to the argon laser beam.

kHz), as shown in Fig. 3. The basic wafers were prepared to produce standard concentrations of metal contaminated, Fe-doped Si, with no other dopant present. For the Fe samples that are annealed we can relate the signal strength with the uniformly distributed dopant concentration, as we had conjectured from Eq. (3). An increase in dopant concentration enhances the carrier recombination probability and this results in a reduction of the carrier lifetime. There is a concomitant reduction in the signal strength in the low frequency regime.[2] From Fig. 3 we are able to clearly determine the differences between annealed samples that are doped from 5×10^{10} to 5×10^{12}. Given the signal-to-noise ratio of the data recovered using PTR, it becomes clear that one can resolve the doping levels to better than an order of magnitude; also shown on this curve are fits based on Eq. (1). Again there is good qualitative agreement between the measured data and theoretical curves, suggesting a minority carrier lifetime on the order of 0.01–0.1 ms for the majority of Fe-doped samples. The nonannealed Fe samples behave like a two-layer system with the doped Fe residing predominantly at the surface, therefore, giving similar signal strengths. A comparison of Figs. 1–3 shows good qualitative agreement between the theory and experiment, the only obvious deviation is in the thermal regime which is indicative that a two-layer model may well be more appropriate.[6]

B. Time-dependent behavior

Additionally, we examined the behavior of the Si sample and annealed Fe samples in the thermal regime, by maintaining a constant modulation frequency, in this case 77 Hz, while monitoring the signal strength as a function of time and for different numbers of exposure. Figures 4 and 5 show that for the Si- and Fe-doped samples the signal magnitude changes if the pump beam is allowed to continually illuminate the same spot on the wafer and that the final signal level is sensitive to the number of exposures. It is interesting to note that the time dependent curves for the first exposure to the laser beam may be fitted with an expression of the form[7]

$$\mathrm{PTR}(t)=A_1(1-A_2\exp(A_3t)\mathrm{erfc}(\sqrt{A_3t})). \tag{6}$$

This indicates that the laser induced temporal effect is diffusive in origin and corresponds to a source term of the form $\exp(A_3t)$. This is evidence that annealing of the surface states is taking place. Using the above equation we are able to predict the $t=\infty$ value, shown in the inset of Fig. 5. It is clear that the $t=\infty$ signal is sensitive to the concentration of metal impurity and therefore to the level of wafer damage. However, the laser beam temperature cannot exceed more than a few degrees and therefore one cannot anticipate any annealing effect on the lattice disorder damage. It may be possible that the extrinsic, i.e., impurity or defect surface states may be altered by charge neutralization, bond reconfiguration, or promotion to another state, by the presence of a photogenerated electron-hole plasma. It may be that the shape of the curve leading to the $t=\infty$ signal, as a function of the numbers of exposure, is indicative of the presence of extrinsic surface states and lattice disorder. The latter would establish the level of the signal strength, whereas the former would

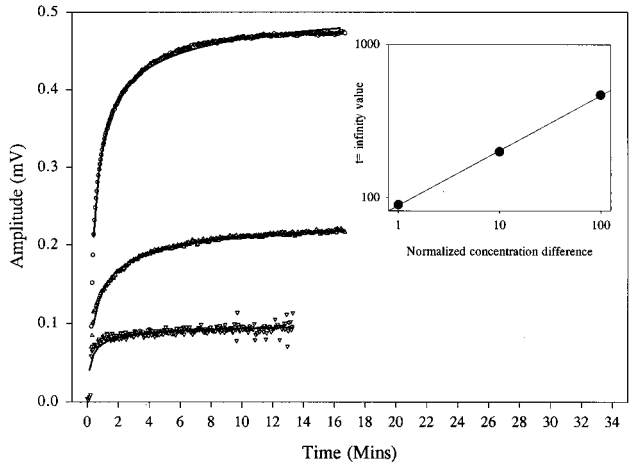

FIG. 5. Time dependent behavior of metal contaminated silicon wafer on first exposure to the pump laser beam, with corresponding theoretical fits using Eq. (6). Inset $t=\infty$ value vs normalized concentration difference showing linear response. Legend: Fe 5×10^{10}+rec. First cycle - ○, Fe 5×10^{11}+rec. First cycle - △, Fe 5×10^{12}+rec. First cycle - ∇.

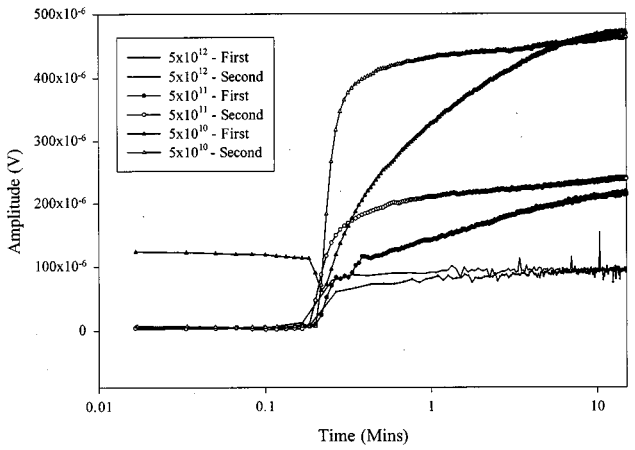

FIG. 6. Time dependent behavior of metal contaminated silicon wafers for various concentrations of Fe on first and second exposure to the pump laser beam, with corresponding departure from the behavior described by Eq. (6).

determine the shape of the curve during the approach towards saturation. Indeed, we observe that for subsequent exposures there is a departure from the behavior of Eq. (6) and a fit cannot be obtained, as seen in Fig. 6. The implication here is that the annealing of the defect center states when completed results in a permanent change in the surface properties of the wafer, although the $t=\infty$ value remains approximately the same in these cases. We are currently making a closer evaluation of this time dependent behavior.

IV. DISCUSSION

We note that the photothermal radiometric technique is a potentially useful approach for nondestructively evaluating the influence of metal-dopant dosage on silicon wafers. The range of metallic contamination is diverse in both the way contamination is introduced and the resulting changes in the response of the Si wafers; therefore, it is necessary to find alternative approaches for nondestructively evaluating wafers, such as the photothermal radiometric measurement. We do not as yet have any independent methods for measuring the carrier lifetimes, but are seeking to address this issue in the near future. To close, we have demonstrated that photothermal radiometry can provide information on both frequency and time dependent behavior of metal contaminated silicon wafers that may prove useful in the wafer manufacturing process.

[1] *Photoacoustic and Thermal Wave Phenomena in Semiconductors*, edited by A. Mandelis (North–Holland, New York, 1987).
[2] A. Othonos, C. Christofides, and A. Mandelis, Appl. Phys. Lett. **69**, 821 (1996).
[3] S. Sheard and M. Somekh, in *Progress in Photothermal and Photoacoustic Science and Technology*, edited by A. Mandelis (Prentice Hall, Englewood Cliffs, NJ, 1994), Vol. II, Chap. 5.
[4] A. Salnick, A. Mandelis, H. Ruda, and C. Jean, J. Appl. Phys. **82**, 1853 (1997).
[5] A. Mandelis, A. Othonos, C. Christofides, and J. Boussey-Said, J. Appl. Phys. **80**, 5332 (1996).
[6] M. Nestoros, Y. Karmiotis, and C. Christofides, J. Appl. Phys. **82**, 6220 (1997).
[7] A. Rosencwaig, ''Thermal Wave Characterization and Inspection of Semiconductor Materials and Devices,'' in *Photoacoustic and Thermal Wave Phenomena in Semiconductors*, edited by A. Mandelis (North–Holland, New York, 1987), Chap. 5.